

Neural Color Transfer between Images *

Mingming He¹†, Jing Liao², Lu Yuan², Pedro V. Sander¹
¹Hong Kong University of Science and Technology, ²Microsoft Research

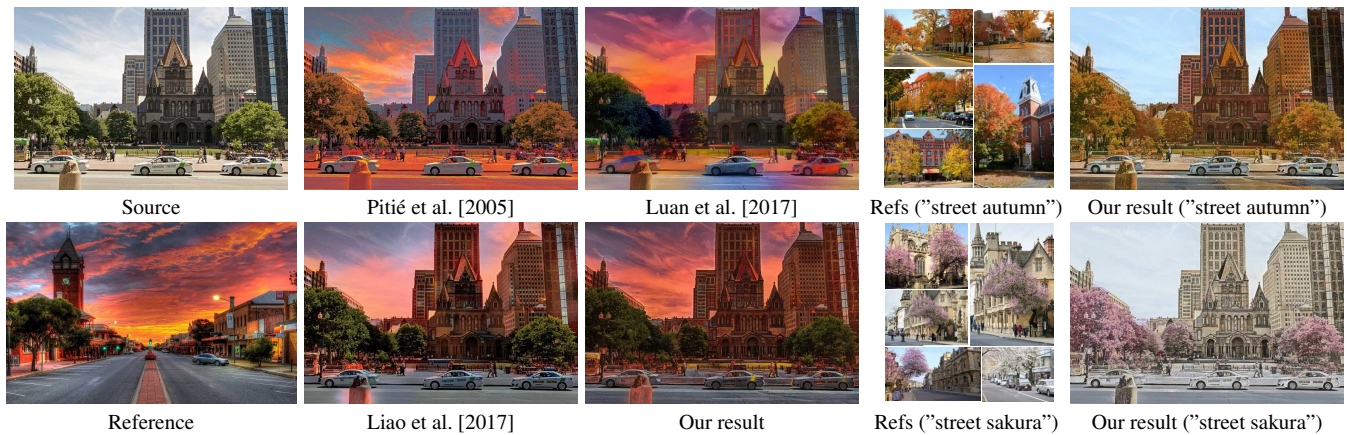


Figure 1: Our method leverages semantically-meaningful dense correspondences between images, thus achieving a more accurate object-to-object color transfer than other methods (left). Moreover, our method can be successfully extended to multiple references (right).

Abstract

We propose a new algorithm for color transfer between images that have perceptually similar semantic structures. We aim to achieve a more accurate color transfer that leverages semantically-meaningful dense correspondence between images. To accomplish this, our algorithm uses neural representations for matching. Additionally, the color transfer should be spatially-variant and globally coherent. Therefore, our algorithm optimizes a local linear model for color transfer satisfying both local and global constraints. Our proposed approach jointly optimizes matching and color transfer, adopting a coarse-to-fine strategy. The proposed method can be successfully extended from “one-to-one” to “one-to-many” color transfers. The latter further addresses the problem of mismatching elements of the input image. We validate our proposed method by testing it on a large variety of image content.

1 Introduction

Color transfer is a long-standing problem that seeks to transfer the color of a reference photograph onto another image. For instance, by appropriately choosing the reference photo, one can make the input image look like it has been taken under a different illumination, time of day, or weather conditions. The method can also be used to artistically retouch color effects.

So far, existing techniques inevitably face some challenges. The work of color transfer originates from global color transformation [Reinhard et al. 2001]. However, such a transform cannot model spatially varying color effects across an image and thus is limited in its ability to match the desired color styles. More expressivity requires spatially variant effects, but it further adds to the challenge of preventing spatial color shifts or distortions. Another challenge is that an accurate transfer should respect the semantics of the scene. For example, in a cityscape as shown in Figure 1, the color of the

buildings should be matched to the buildings, sky to sky, and so on. It is unacceptable to transfer the sky color to the buildings.

In this paper, we describe a new algorithm for color transfer between images. Our approach is applicable for cases where images may be very different in appearance but semantically similar. Essentially, the images should be of the same type of scene containing elements of the same classes, e.g., cityscape scenes featuring buildings, streets, trees, and cars. Figure 1 shows such semantically similar pairs. We aim to achieve precise local color transfer from semantically similar references, which is essential to automatic and accurate image editing, such as makeup transfer and creating time-lapses from images.

To achieve this accurate transfer, we must establish semantically-meaningful dense correspondences between input images. Due to large variations in appearance, matching methods based on low-level features (e.g., intensity, Gabor wavelet, SIFT, or SSIM) may fail. To enable high-level semantic matching, some methods require segmentation [Luan et al. 2017], or user specifications [An and Pellacini 2010], but they are not quite effective in building precise pixel-to-pixel correspondences.

Inspired by Liao et al. [2017; 2016], our approach leverages neural representations (e.g., convolutional features of pre-trained VGG-19 [Simonyan and Zisserman 2014]) for dense semantic matching.

After each pixel obtains the matched color from the reference, we apply local color transfer in the image domain instead of the feature space. This avoids undesired distortions in edges or detailed patterns. The local color transfer considers a linear transform at every pixel, enforcing both local smoothness and non-local constraints to avoid inconsistencies.

Both steps are performed alternatively in a coarse-to-fine manner and thus mutually contribute to each other’s results at each layer: the NNF is used to guide the local color transfer at the current CNN layer, and then the transferred result, whose appearance becomes much closer to the reference, allows the NNF to be refined at the next CNN layer.

*Supplemental material: https://liaojing.github.io/html/data/color_supp.pdf.

†This work was done when Mingming He was an intern at MSR Asia.

Our other key contribution is a multiple-reference color transfer solution, which addresses the issue of missing semantically equivalent elements in the reference. If a single reference image lacks a visible sky (e.g., Figure 1), it could cause an inaccurate color transfer from other elements to the sky. This algorithm extends *one-to-one* to *one-to-many* NNF search, and uses a Markov Random Field (MRF) optimization to obtain the piecewise smooth NNF. The proper reference images can come from either tagged personal photo albums or image search engine results with specific keywords such as “street autumn” or “cityscape night”.

Our major technical contributions are:

1. We present a new “neural color transfer” method, which jointly optimizes matching in deep feature domain and local color transfer in image domain.
2. We present a new local color transfer model, which is based on a pixel-granular linear function, avoiding local structural distortions and global incoherency by enforcing both local and global constraints.
3. We extend *one-to-one* to *one-to-many* color transfer, which effectively avoids content mismatching between images.

We show how our neural color transfer technique can be effectively applied to a variety of real scenarios. Our technique can also be applied to transfer colors to a gray image, known as the colorization problem.

2 Related Work

Global Color Transfer. Global color transfer algorithms apply a spatially-invariant color transformation to an image, such as global color moves (e.g., sepia) and tone curves (e.g., high or low contrast). The seminal work by Reinhard et al. [2001] matches the mean and standard deviation between the input and the reference in the $l\alpha\beta$ color space. Freedman et al. [2005] transfer the full 3D color histogram using a series of 1D histograms. Freedman et al. [2010] compute the transfer for each histogram bin with the mean and variance of pixel values in the bin, which compromises between mean-variance based methods and histogram based methods. These methods only consider global color statistics, ignoring the spatial layout.

HaCohen et al. [2011] estimate and utilize reliable local correspondences between images for estimating the global non-linear color mapping. Their results are compelling but the dependence on the input image pairs is high. For example, two photos should be from the same scene with variations in view, color, and illumination.

Local Color Transfer. Local color transfer algorithms based on spatial color mappings are more expressive and can handle a broad class of applications [Bae et al. 2006; Shih et al. 2013; Shih et al. 2014; Sunkavalli et al. 2010; Laffont et al. 2014]. Local correspondences are often in high demand for transfers. Some methods require sparse correspondence guidance from the user input [An and Pellacini 2010; Welsh et al. 2002]. Other approaches consider an automatic way to estimate local correspondences, for example, region-by-region color transfer [Yoo et al. 2013; Tai et al. 2005; Arbelot et al. 2017], depending on automatic image segmentation algorithms. Such matches are not yet precise enough, causing some pixels to be transferred to inaccurate colors.

To handle very drastic variations in color appearance between image pairs (e.g., photos from different times of day), some methods [Shih et al. 2013; Laffont et al. 2014] consider an additional pair of well-aligned images (one resembling the input source and

the other resembling the input reference) as the bridge for the transfer. Through such a bridging image pair, a locally linear color model is estimated and then applied to the input image pair.

Deep Color Transfer. Recently, deep neural networks have provided a good representation to directly establish semantically-meaningful correspondence between visually different image pairs. The remarkable work of “deep photo style transfer” [Luan et al. 2017] extends neural style transfer [Gatys et al. 2015] to photo-realistic transfer by enforcing local color affine constraints in the loss function. Their region-to-region matching relies on semantic segmentation [Chen et al. 2016] of the image pairs.

Our work is inspired by the work of “deep image analogy” [Liao et al. 2017], which estimates the semantically dense correspondences between two images based on deep features. However, our work has three key differences from “deep image analogy” for color transfer. First, our approach jointly optimizes matching and local color transfer, which improves matching used for the transfer over Liao et al. [2017] where the separative optimization is employed. Second, to transfer color, our approach optimizes the linear transform model satisfying local and global coherence constraints while theirs just swaps the low-frequency bands of two input images. Third, our approach can be extended to *one-to-many* color transfer, which effectively avoids content-mismatching in *one-to-one* transfer [Liao et al. 2017].

Multi-reference Color Transfer. Choosing a proper reference for color transfer is crucial when using a single reference. To ease the burden of reference selection, some methods adopt multiple references. Liu et al. [2014] search and cluster a collection of references with similar color styles from the Internet by providing a text query, (e.g., “winter”, “desert”). Lee et al. [2016] automatically learn reference ranking for a given input using a large photo collection, and select a diverse subset of matching references for the transfer. Both methods finally apply the global color transfer after getting multiple references. To achieve more precise local transfer, Khan et al. [2016] allow user to manually give some correspondence guidance between input and multiple references, and then use the locally linear embedding (LLE) method [Roweis and Saul 2000] to propagate the guidance.

Deep networks have recently been introduced to the task of color transfer. Yan et al. [2016] learn a highly non-linear color mapping function for automatic photo adjustment by taking the bundled features as the input layer of a deep neural network. Isola et al. [2016] train generative networks on a dataset of paired images for image appearance transfer, including colors. Zhu et al. [2017] loosen the constraints to unpaired images. These methods take several hours to train a single color style. The network-generated results are low resolution and often suffer from checkboard artifacts caused by deconvolution layers [Odena et al. 2016]. Instead, our method only uses features from pre-trained networks for matching. We can support high-quality transfer of various color styles without training.

Colorization. Colorization deals with the process of adding color to a grayscale image. Early approaches to address this issue rely on user scribbles and extend them via optimization across similar regions [Levin et al. 2004]. Recently, deep learning algorithms have been used for automatic image colorization [Zhang et al. 2016; Iizuka et al. 2016], but these methods have to learn image statistics from large extensive datasets. Given one reference image instead of user input, some automatic methods transfer the chrominance between pixels containing similar statistics [Arbelot et al. 2017; Welsh et al. 2002]. Our method is also applicable to colorization using reference images of the same class.

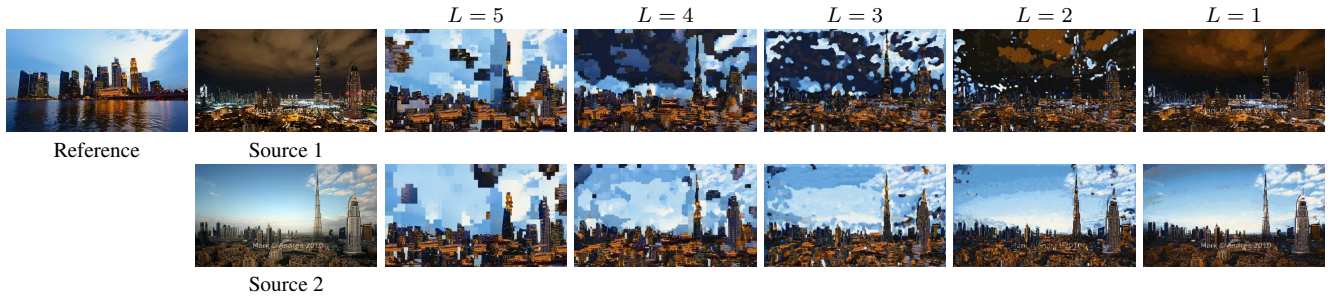


Figure 2: Matching results from the NNF search with different level features $reluL_1$, $L = 5, \dots, 1$ in VGG19. We show two transfer pairs (all from [Shih et al. 2013]): one has more distinct colors (upper row) and another has similar colors (lower row). It is clear that NNFs based on high-level features (e.g., $L = 5$) are less sensitive to color appearance than NNFs based on low-level features (e.g., $L = 1, 2$).



Figure 3: Comparison with performing color transfer directly in the feature domain. (a) Mapped features in VGG19 $relu3.1$ layer; (b) Images deconvolved from (a); (c) Close-up patches from (b); (d) Corresponding patches of performing color transfer in the image domain as described in Section 3.2; (e) Corresponding patches from the source image.

3 Method

Our goal is to apply precise local color transfer based on the established dense correspondences between the source image S and the reference image R . In our scenario, the two input images share some semantically-related content. To achieve this goal, we face two challenges.

First, it is difficult to directly build correspondence between both images since they may differ in color appearance. To address this problem, we leverage neural representations for matching (in Sec. 3.1). Deep features from CNN encode the image gradually from low-level details to high-level contents. High-level features in neural networks (e.g., $relu5_1$ layer in vgg19) can be used to match semantically similar objects ignoring color differences. As shown in Figure 2, blue-to-blue sky image pair (reference and source 2) and blue-to-dark sky image pair (reference and source 1) achieve very close matching results at the coarsest level ($L = 5$). Low-level features (e.g., $relu1_1$ layer in VGG19) are sensitive to color appearance and thus fail to match objects with semantic similarity but different colors, e.g., matching result of blue-to-dark sky image pair at the finest level ($L = 1$) (see the 1st row of Figure 2). Besides, we observe that matching accuracy could be improved from high-level to low-level features when colors of both image pairs are similar (see the 2nd row of Figure 2). This inspired us to develop a coarse-to-fine strategy to alternatively optimize the nearest-neighbor fields (NNFs) and color transfer. Thus, the two steps are mutually beneficial.

Second, for color transfer, we cannot directly deconvolve the mapped features from the reference to reconstruct the image as done by [Liao et al. 2017]. Such a direct reconstruction from neural representations introduces local structure distortions, and check-board (or ringing) artifacts, as shown in Figure 3. These artifacts preclude us from producing a photo-realistic and high-quality color

transfer. Instead, we apply local color transfer in the image domain (in Sec. 3.2).

Figure 4 shows our system pipeline. At every level L , we first match the reference R to the intermediate source \tilde{S}^{L+1} (initially \tilde{S}^6 is the source S) using $reluL_1$ layer of VGG19 to get bidirectional NNFs in the feature domain and use the NNFs to reconstruct a color guidance G^L . Next, we estimate the local color transfer function between the downscaled version of source S^L and G^L , upscale the transformation, and apply it to S in the image domain. The two steps alternate and mutually assist one another: the NNFs help obtain a more accurate local color transfer, while the color transferred result \tilde{S}^L serves as the source also helps refine the matching in next level $L - 1$, since \tilde{S}^L has much more similar colors to the reference than the original source S . Both intermediate results (NNFs and \tilde{S}^L) serve as the bridge between both matching and color transfer which occur at different domains. Following this strategy, both steps are gradually refined.

3.1 Nearest-Neighbor Field Search

Given the intermediate source \tilde{S}^{L+1} and the reference R at level L ($L = 5, \dots, 1$), our NNF search step builds the bidirectional correspondences between them. Here, \tilde{S}^{L+1} is the color transferred result (with the same resolution to the source S) from the coarser level $L + 1$ when $L < 5$. At the coarsest level $L = 5$, \tilde{S}^{L+1} is initialized as S .

In view of the difficulty of building correct correspondences between \tilde{S}^{L+1} and R with potentially big variances in their appearance. We perform NNF search in the deep feature domain. Since the CNN will almost keep the spatial relationship of input images, the NNFs computed in the feature domain can be used in the image domain. To do so, we first feed the \tilde{S}^{L+1} and R to the VGG19 network [Simonyan and Zisserman 2014] pre-trained on the ImageNet database [Russakovsky et al. 2015] for object recognition. We then extract their feature maps in $reluL_1$ layer, labeled as F_S^L , F_R^L respectively for \tilde{S}^{L+1} , R . Each feature map is a 3D tensor with $width \times height \times channel$, and its spatial resolution is $\frac{1}{2^{L-1}}$ of the input image.

The mapping function $\phi_{S \rightarrow R}^L$ from F_S^L to F_R^L is computed by minimizing the following energy function:

$$\phi_{S \rightarrow R}^L(p) = \arg \min_q \sum_{x \in N(p), y \in N(q)} (\|\bar{F}_S^L(x) - \bar{F}_R^L(y)\|^2) \quad (1)$$

where $N(p)$ is the patch around p . We set the patch size to 3×3 at

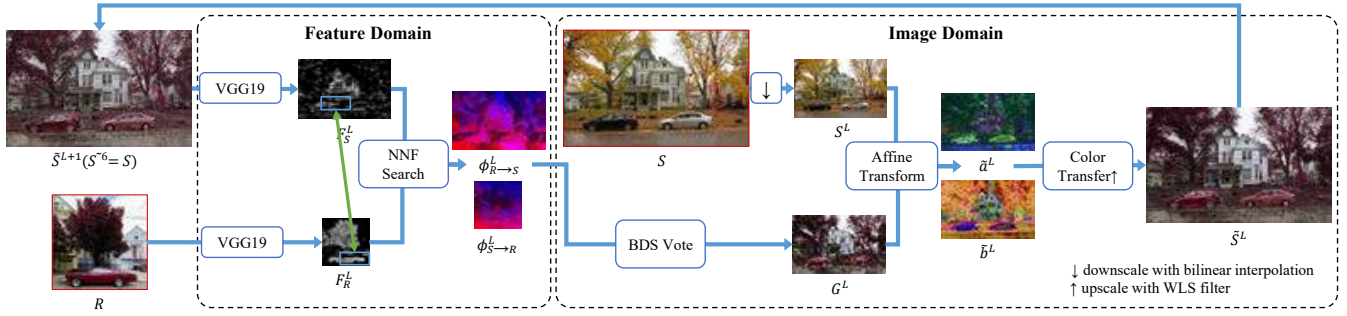


Figure 4: System pipeline. We perform matching in the feature domain, and apply local color transfer in the image domain. The two inputs are S and R , and the final output is \tilde{S}^1 . At every level L , the intermediate color transferred result \tilde{S}^L is used as the source for matching of the next level $L - 1$.

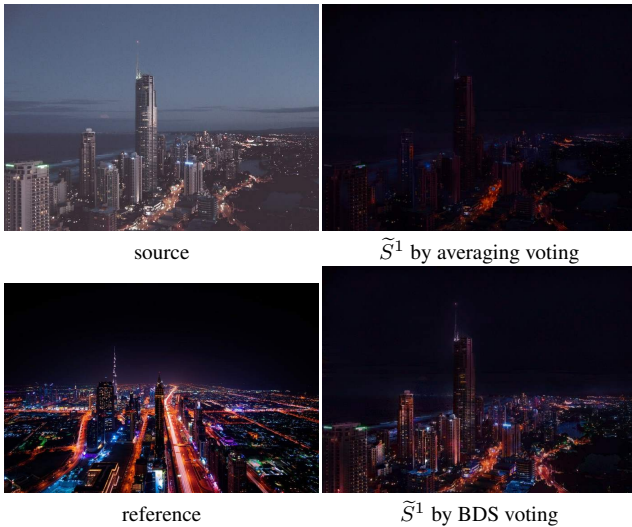


Figure 5: Comparisons between results by average voting and by BDS voting.

each level. For each patch around position p in the source feature F_S^L , we find its nearest neighbor patch around $q = \phi_{S \rightarrow R}^L(p)$ in the reference feature F_R^L . $F(x)$ in Equation (1) is a vector representing all channels of feature map F at position x . We use normalized features $\bar{F}^L(x) = \frac{F^L(x)}{|F^L(x)|}$ in our patch similarity metric, because relative values are more meaningful than absolute values in networks.

The reverse mapping function $\phi_{R \rightarrow S}^L$ from F_R^L to F_S^L is computed in the same way as (1) by exchanging S and R . Both mappings $\phi_{S \rightarrow R}^L$ and $\phi_{R \rightarrow S}^L$ can be efficiently optimized with the PatchMatch algorithm [Barnes et al. 2009], which also implicitly achieves smoothness through aggregation of overlapping patches.

The bidirectional correspondences allow us to use Bidirectional Similarity (BDS) voting [Simakov et al. 2008] to respectively reconstruct the guidance image G^L and the feature map F_G^L . G^L will serve as the guidance for color transfer in the next step, while F_G^L will be used to measure matching errors $e^L(p) = \|\bar{F}_S^L(p) - \bar{F}_G^L(p)\|^2$ in Equation (4). The BDS voting is performed to average the pixel colors/features from all overlapping nearest-neighbor

patches in the reference R^L / F_R^L through the forward NNF $\phi_{S \rightarrow R}^L$ and the backward NNF $\phi_{R \rightarrow S}^L$. The forward NNF enforces coherency (i.e., each patch in the source can be found in the reference), while the backward NNF enforces completeness (i.e., each patch in the reference can be found in the source). By enforcing both coherency and completeness, BDS voting can achieve result more similar to the reference than average voting with solely forward NNF, as shown in Figure 5.

We show the NNFs $\phi_{R \rightarrow S}^L$, and guidance image G^L ($L = 5, \dots, 1$) gradually refined from the coarse layer to the fine layer in Figure 6.

3.2 Local Color Transfer

Given the guidance image G^L at each level L , we propose a new local color transfer algorithm, which changes the colors of the source S to better match those of G^L . Then, we may get the color transferred result \tilde{S}^L . Since S and G^L have different resolution at the coarse levels ($L > 1$), it is impossible to build in-place correspondence between S and G^L . Instead, we downscale S to S^L to match the resolution of G^L , estimate the color transfer function from S^L to G^L , upscale the function parameters with an edge-preserving filter, and finally apply it to the full-resolution S to get the intermediate transferred result \tilde{S}^L , which is then used for the NNF search at the next level.

For every pixel p in S^L , we model the local color transfer as a linear function of each channel in CIELAB color space, which is denoted by

$$\mathcal{T}_p^L(S^L(p)) = a^L(p) \times S^L(p) + b^L(p). \quad (2)$$

The goal is to estimate linear coefficients $a^L(p)$ and $b^L(p)$ for each pixel p , making the transferred result $\mathcal{T}_p^L(S^L(p))$ visually similar to the guidance $G^L(p)$.

We formulate the problem of estimating \mathcal{T}^L by minimizing the following objective function consisting of three terms:

$$E(\mathcal{T}^L) = \sum_p E_d(p) + \lambda_l \sum_p E_l(p) + \lambda_{nl} \sum_p E_{nl}(p), \quad (3)$$

where λ_l and λ_{nl} are tradeoff weights (by default, $\lambda_l = 0.005$ and $\lambda_{nl} = 0.5$).

The first data term E_d makes the color transfer result similar to the guidance G^L :

$$E_d(p) = (1 - \bar{e}^L(p)) \|\mathcal{T}_p^L(S^L(p)) - G^L(p)\|^2, \quad (4)$$

¹ R^L is the same resolution as F_R^L , downsampled from the reference R

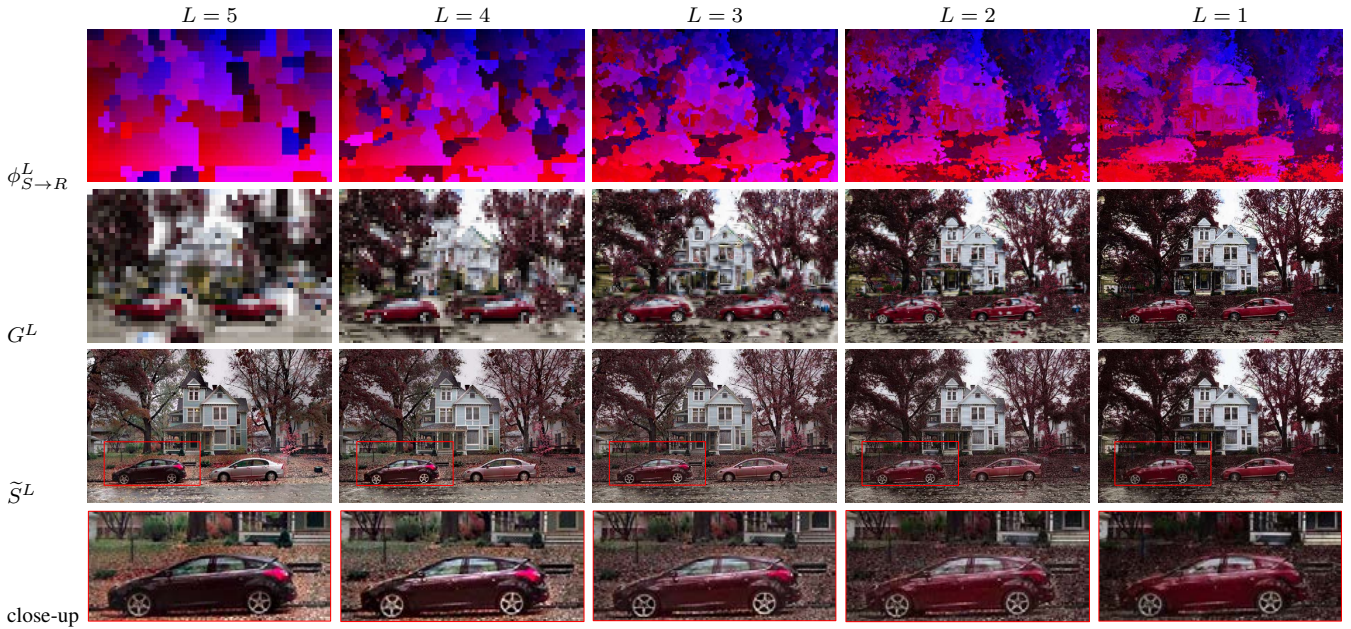


Figure 6: Both NNF field $\phi_{S \rightarrow R}^L$ and color transfer results \tilde{S}^L are gradually refined from top to bottom layer.

where the normalized matching error \bar{e}^L is used as the weight to give high confidence to well-matched points.

The second smoothness term E_l encourages adjacent pixels to have a similar linear transform:

$$E_l(p) = \sum_{q \in N_8(p)} \omega(p, q) (\|a_p^L - a_q^L\|^2 + \|b_p^L - b_q^L\|^2), \quad (5)$$

where $N_8(p)$ is the 8-connected neighbors at p , and the weight $\omega(p, q) = \frac{\exp \|S^L(p) - S^L(q)\|}{\sum_{q' \in N_8(p)} \exp \|S^L(p) - S^L(q')\|}$ is determined by the color similarity between $S^L(p)$ and its neighbors $S^L(q)$. It encourages pixels with similar color within the local window 3×3 to share the same transform.

The last term E_{nl} enforces the non-local constraint to penalize global inconsistency. It is based on the assumption that pixels with similar colors in the source should get identical transferred colors in the result. The constraint has been successfully applied in matting [Chen et al. 2013], intrinsic image decomposition [Zhao et al. 2012] and colorization [Endo et al. 2016]. We consider the similarity of both color and semantics to compute the non-local term. We first apply K-means to get 10 clusters in the highest-level (most semantic) features F_S^5 . In each cluster, we find k nearest neighbors in the color space for each pixel p of S^L , labeled as $K(p)$ (where $k = 8$). The non-local smoothness term is then defined as:

$$E_{nl}(p) = \sum_{q \in K(p)} \omega(p, q) \|\mathcal{T}_p^L(S^L(p)) - \mathcal{T}_q^L(S^L(q))\|^2, \quad (6)$$

where $\omega(p, q)$ is the same as in Equation (5). With these non-local constraints, artifacts are reduced and color transfer are thus more globally consistent as shown in Figure 7.

The closed-form solution of Equation (3) is very costly due to the irregular sparse matrix structure. Instead, our alternative solution first estimates a good initial guess and then performs a few conjugate gradient iterations, which achieves much faster convergence for \mathcal{T}^L .



Figure 7: Comparison with and without non-local constraint.

We initialize \mathcal{T}^L by applying the global color transformation method [Reinhard et al. 2001] on every local patch. Specifically, taking a patch $N(p)$ centered at pixel p in S^L and in G^L , we estimate the initialized \mathcal{T}^L by matching the mean μ and standard deviation σ of the patch pair in each color channel separately:

$$\begin{aligned} a^L(p) &= \sigma_{G^L(N(p))} / (\sigma_{S^L(N(p))} + \epsilon) \\ b^L(p) &= \mu_{G^L(N(p))} - a^L(p) \times \mu_{S^L(N(p))}, \end{aligned} \quad (7)$$

where ϵ is used to avoid dividing zero ($\epsilon = 0.002$ for color range $[0, 1]$). We set the patch size to be 3×3 for all layer.

The above parameters $a^L(p)$ and $b^L(p)$ are estimated in low resolution. We apply the WLS filter [Farbman et al. 2008] to upsample them to the full-resolution, which is guided by source image S , obtaining a_{\uparrow}^L and b_{\uparrow}^L . The two weights used in the WLS filter are set

ALGORITHM 1: Neural Color Transfer Algorithm

Input : Source image S and reference image R .**Initialization:**

$$\tilde{S}^6 = S.$$

for $L = 5$ **to** 1 **do** **NNF search** (Section 3.1): $F_S^L, F_R^L \leftarrow$ feed \tilde{S}^{L+1}, R to VGG-19 and get features. $\phi_{\tilde{S} \rightarrow R}^L \leftarrow$ map F_R^L to F_S^L by Eq. (1). $\phi_{R \rightarrow \tilde{S}}^L \leftarrow$ map F_S^L to F_R^L . $G^L \leftarrow$ reconstruct S^L with R^L by BDS voting. **Local color transfer** (Section 3.2): $a^L, b^L \leftarrow$ optimize local linear transform from S^L to G^L

by minimizing Eq. (3).

 $a_{\uparrow}^L, b_{\uparrow}^L \leftarrow$ upscale and a^L, b^L with WLS filter guided by S . $\tilde{S}^L \leftarrow$ transfer the color of S by Eq. (8).**end****Output:** Color transferred result \tilde{S}^1 .

to $\alpha = 1.2$ and $\lambda = 0.032$ by default.

$$\tilde{S}^L(p) = a_{\uparrow}^L(p) \times S(p) + b_{\uparrow}^L(p), \quad \forall p \in \tilde{S}^L. \quad (8)$$

The result \tilde{S}^L (in Figure 6) is then used for the NNF search in the next level $L - 1$ to update the correspondences. Once the finest layer $L = 1$ is reached, \tilde{S}^1 is our final output.

3.3 Algorithm and Performance

The pseudo code of our implementation is listed in Algorithm 1. Our core algorithm is developed in CUDA. All of our experiments are conducted on a PC with an Intel E5 2.5GHz CPU and an NVIDIA Tesla K40c GPU. The runtime is about 80 seconds for input images with an approximate resolution of 700×500 . There are two bottlenecks in the processing: the deep PatchMatch (40 seconds), which needs to compute patch similarities on hundreds of feature channels, and the optimization of local color transform (30 ~ 50 seconds), which requires solving large sparse linear equations.

4 Multi-reference Neural Color Transfer

Our algorithm is extendable to multi-reference color transfer. This avoids the difficulty of having to choose a single proper reference image that is suitable for all portions of the source image. The *one-to-one* matching (described in Section 3.1) can be extended to *one-to-many* matching as follows.

Given multiple references $R_i (i = 1, \dots, n)$, we compute the bidirectional NNFs between \tilde{S}^{L+1} and every reference R_i at each level L , then reconstructing each guidance image G_i^L (shown in Figure 8) using obtained NNFs. Next, we combine these guidance images into a single G^L , which requires selecting the best one from n candidates $G_i^L (i = 1, \dots, n)$ at each pixel p . The selection criteria include: (1) how well the reference is matched to the source; (2) how similar the resulting pixel color is compared to the majority of guidance colors; (3) how consistently the indices are selected between the pixel and its neighborhoods. Based on these criteria, we compute the index selection map I^L by minimizing the following objective function:

$$\mathcal{E}(I^L) = \sum_p \mathcal{E}_e(p) + \beta_m \sum_p \mathcal{E}_m(p) + \beta_s^L \sum_{p, q \in N_4(p)} \mathcal{E}_c(p, q), \quad (9)$$

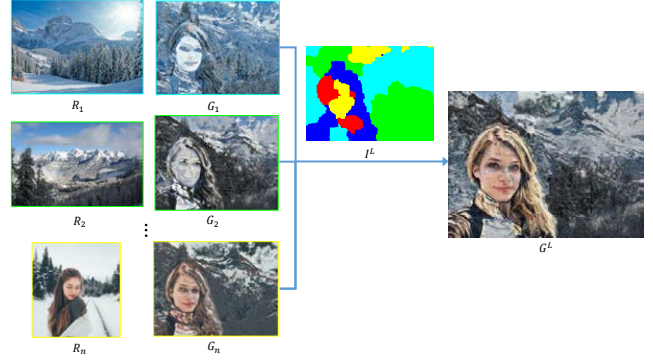


Figure 8: In a multiple-reference scenario, the image G^L used to guide color transfer is merged from multiple guidances $G_i^L, i = 1, \dots, n$ reconstructed with bidirectional NNFs.

where $N_4(p)$ denotes the 4-connected neighborhood of p , $\beta_s^L = 0.04 \times 2^{5-L}$ and $\beta_m = 0.2$.

Let E_i^L be the error map of i -th NNFs. The first term measures matching error from R_i at each pixel.

$$\mathcal{E}_e(p) = E_i^L(p) \quad (10)$$

The second term measures the difference between each guidance color and the median of the guidance colors at every pixel:

$$\mathcal{E}_m(p) = \|G_i^L(p) - \text{median}(G_i^L(p))\|^2 \quad (11)$$

The third term measures local smoothness, which encourages neighboring features in the combination result to be consistent :

$$\mathcal{E}_c(p, q) = \|\overline{F}_{G_i}^L(p) - \overline{F}_{G_j}^L(p)\|^2 + \|\overline{F}_{G_i}^L(q) - \overline{F}_{G_j}^L(q)\|^2, \quad (12)$$

where $i = I^L(p)$ and $j = I^L(q)$.

Equation (9) formulates a Markov Random Field (MRF) problem over the 2D spatial domain, which can efficiently solved by using multi-label graph cut [Kolmogorov and Zabini 2004]. To obtain a good initialization for the optimization, $I^L(p)$ is initialized by minimizing only the data terms ($\mathcal{E}_e(p)$ and $\mathcal{E}_m(p)$). After solving for I^L , we obtain a single guidance image G^L by simply merging all results from multiple references, *i.e.*, $G^L(p) = G_{I^L(p)}^L(p)$. Then, G^L is used for the following step of local color transfer described in Section 3.2. The right image of Figure 8 shows the optimal reference index map I^L and the merged guidance G^L . Compared to single-reference matching, it can effectively solve the content-mismatch problem in situations where it is difficult to find a suitable single source.

5 Results and Comparisons

In this section, we show the application results of our method, including single-reference color transfer, color transfer with multiple references or keywords, and colorization. More comparisons and results can be found in our supplemental material.

5.1 Single-Reference Color Transfer

To validate our approach on color transfer, we first discuss visual comparisons with previous works in global, local, and deep color transfer, and then report statistics of our conducted user study.

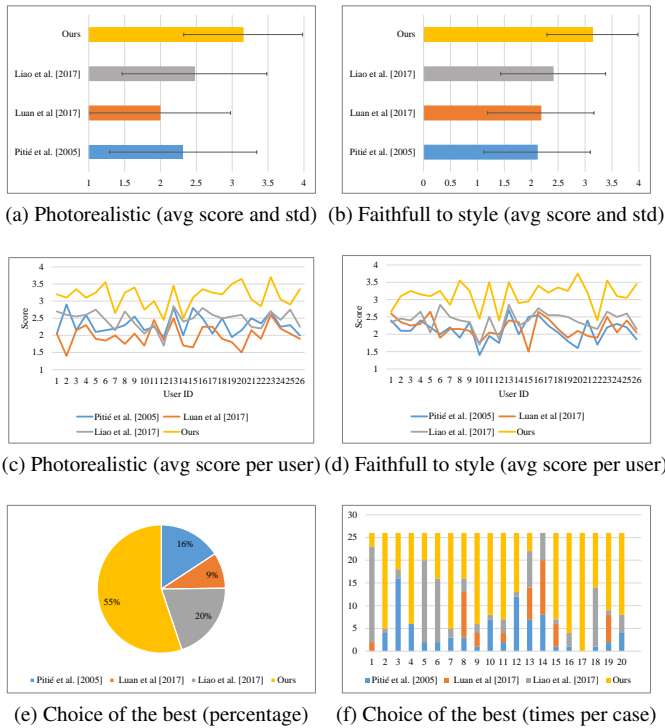


Figure 9: User study results.

In Figure 10, we compare our method with global color transfer methods. Reinhard et al. [2001] and Pitié et al. [2005] only match the global color statistics between the source image and the target image for the transfer, thus limiting the ability to conduct more sophisticated color transformations. For example, in the first result, the house is rendered in blue matching the color of the sky. In contrast, our transfer is local and capable of handling semantic object-object color transfer.

The NRDC method [HaCohen et al. 2011] is based on a small number of reliable matches to estimate the global color mapping function, so it achieves a better transfer result than Pitié et al. [2005]. However, NRDC fails to match two different scenes for the color transfer (e.g., top two rows of Figure 10). As for the two images with the same scene which are suitable for NRDC, (e.g., bottom two rows of Figure 10), our color transfer relies on much denser matching than NRDC, and applies local transformation instead of global, so our transfer produces more accurate results with fewer artifacts than NRDC in local regions, like women’s shirt in the first example and wall in the second one.

We compare our method with the local color transfer methods [Shih et al. 2013; Laffont et al. 2014] in Figure 11. These two algorithms depend on an additional pair of examples (e.g., Reference 1 and Reference 2) which are aligned but have different color styles for the transfer. In contrast, ours directly learns the color from the reference image (i.e., ref2). Therefore, our results look more faithful to the reference colors than theirs. Moreover, our method is more flexible in practice since it does not require an additional aligned pair for the transfer.

In Figure 14, we compare with two recent color transfer methods based on CNN features [Luan et al. 2017; Liao et al. 2017]. The method of Luan et al. [2017] matches the global statistics of deep features (Gram Matrix) and guarantees region-to-region transfer via segmentation masks. One type of noticeable artifact in their results

is posterization, which is visible in the bicycle in the 6th row and the cloud in the last row of Figure 14. Liao et al. [2017] also find dense correspondence between two images based on deep features, yielding results that are more similar to ours. However, unlike their approach which first does matching and then transfers local colors, our method performs joint matching and color transfer, which can align two images better for the color transfer, resulting in fewer ghosting artifacts in the results. This is clearly shown in the mountain area (1st row in Figure 12) and tree area (3rd row in Figure 12). Moreover, their color transfer only exchanges low-frequency color bands; while our linear model considers all-frequency color bands. Thus ours can generate results more faithful to the reference. For example, in the second row of Figure 12, though the guidance images (warped references) of two methods are similar, our color-transferred results are better at reproducing the contrast in the reference.

Moreover, our method is effective in transferring effects like makeup or photographer styles from one portrait to another. Compared to the methods specifically focusing on portraits and very specific kinds of effects, ours can generate comparable results as shown in Figure 13, but without requiring extra inputs of the pair before and after makeup (Tong et al. [2007]), face landmarks (Shih et al. [2014] and Tong et al. [2007]) or matting (Shih et al. [2014]).

User Study. We conduct a user study to evaluate our color transfer work in terms of photorealism and faithfulness to reference style. We compared the following techniques: Pitié et al. [2005], Luan et al. [2017], Liao et al. [2017] and ours in the study. We present the results of four methods to participants in a random order and ask them to score images in a 1-to-4 scale from “definitely not photorealistic” to “definitely photorealistic” for question 1, from “definitely not faithful to the reference” to “definitely faithful to the reference” for question 2, and select the best one considering both criteria for question 3. We use 20 different scenes for each of the four methods and collect the responses from 26 subjects. The examples are randomly selected from the test cases of HaCohen et al. [2011; 2017; 2014].

Figure 9(a)(b) demonstrates the average score and standard deviation of each method. For photorealism and faithfulness, ours and Liao et al. [2017] are ranked 1st and 2nd respectively. Luan et al. [2017] perform worst in photorealism, since it often produces posterization (cartoon-like) effects; while Pitié et al. [2005] perform the worst in faithfulness to style, since global transfer limits present a variety of styles. Figure 9(c)(d) shows the average score given by every user. Ours is consistently better than others in both photorealism and faithfulness among all users. We further conduct repeated-measures ANOVAs on the collected data, and it shows the differences between the four methods from these two aspects are all significant ($p < 0.005$). We also use simple contrasts to compare each method against our method among all 520 choices (26 subjects by 20 cases). For photorealism, users prefer ours over Pitié et al. [2005] (64.04% better, 16.54% equal), Liao et al. [2017] (75.20% better, 11.16% equal) and Luan et al. [2017] (61.73% better, 14.80% equal). For style fidelity, choices prefer ours over Pitié et al. [2005] (72.77% better, 12.69% equal), Luan et al. [2017] (70.96% better, 10.77% equal) and Liao et al. [2017] (65.19% better, 15.19% equal).

Since color transfer quality depends on both photorealism and style fidelity. We examine the subject’s preferred result considering both criteria. The pie chart on Figure 9(e) shows the percentage of each method selected as the best. Our algorithm is the top overall selection over the other three methods on 55% of the time. Figure 9 (f) gives the detailed numbers of how many times each method is selected as the best in each case. It shows that more users prefer ours

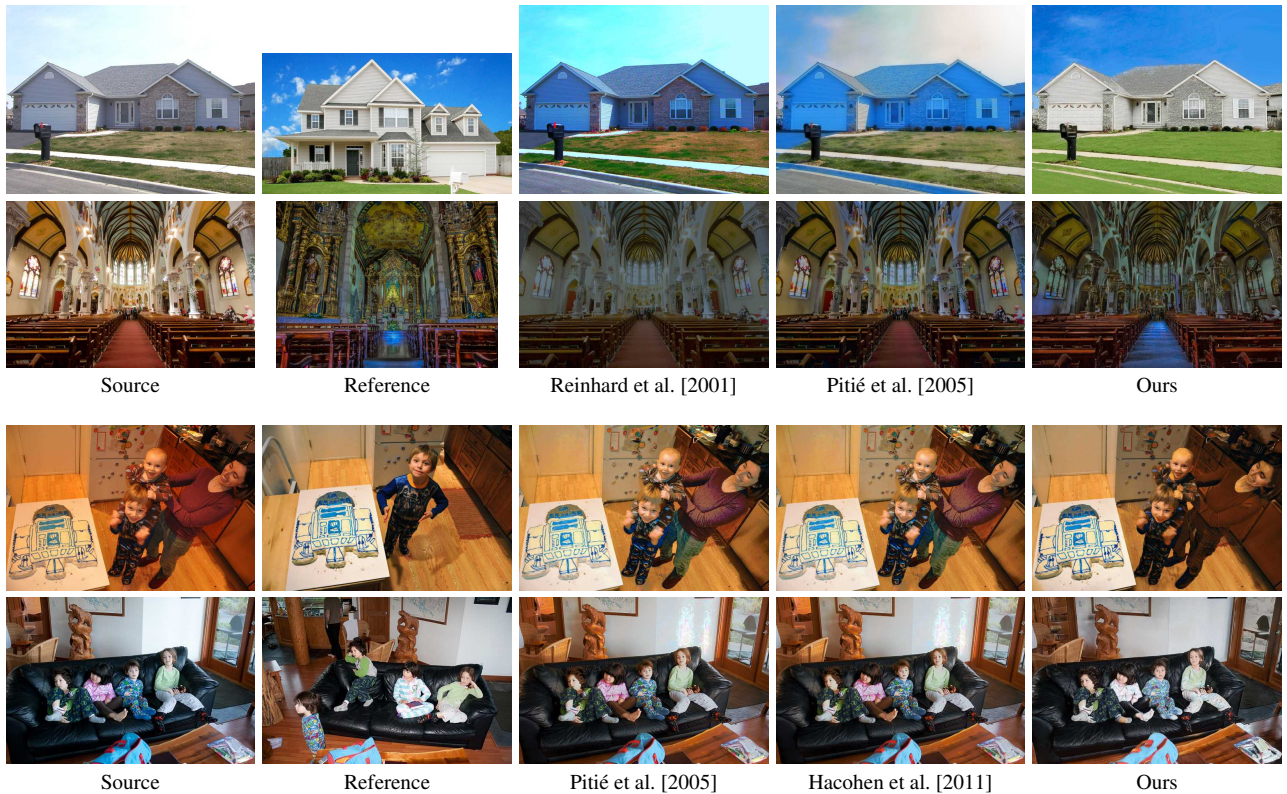


Figure 10: Comparison with global color transfer methods. Examples are from Luan et al. [2017] (top two) and Hacoheh et al. [2011] (bottom two).

over Pitié et al. [2005] (17 cases vs 3 cases), Luan et al. [2017] (17 cases vs 3 cases), and Liao et al. [2017] (14 cases vs 6 cases).

5.2 Multi-Reference Color Transfer

In all single-reference color transfer methods, reference selection is crucial to achieving satisfactory results. Our method fails to transfer correct colors and yields an unnatural appearance in the regions where no proper color guidance can be found in the reference. This problem can be addressed by introducing multiple references. For example, in the bottom row of Figure 16, the sky color is incorrect because the single reference does not contain the sky, but it is correct with multiple references, some of which containing the sky.

Our multi-reference approach allows the user to provide keywords for controlling the color transfer, e.g., “restaurant night” in the first row of 15. “restaurant” describes the content in source images, and “night” defines the desired style. To automatically obtain multiple references for the transfer, these keywords are used to retrieve images through a search engine (e.g., Google Images). We collect the top 50 search results as candidates. Naturally, these images may have a wide variety of color styles as well as outliers. To select a set of images with consistent colors, for each candidate image, we compute its normalized histogram in the HSV color space and select the most representative one with a minimum L_2 histogram distance to all others. Then we choose the closest subset of 5 images to the representative one as the references for transfer. Compared with Autostyle [Liu et al. 2014] which uses a global transfer, our approach performs a local transfer and thus requires more keywords in order to describe both content and style. However, it allows us to produce a more precise color transfer than Autostyle [Liu et al. 2014]. Cycle-GAN [Zhu et al. 2017] also allows transferring a

specific style (e.g., “winter”) to a given source without selecting the reference by leveraging network training on large datasets. Compared to theirs, our method is more flexible to test different styles without retraining. And our results have fewer checkerboard artifacts, as shown on the bottom two rows of 15.

5.3 Colorization

We can also use our method for colorization of gray-scale images. We simply provide color references in the desired style in order to colorize our input gray-scale image. Figure 17 shows some colorization results.

6 Concluding Remarks

In this paper, we demonstrate a new algorithm for locally transferring colors across semantically-related images. It not only handle single-reference transfer, but can also be adapted to multi-reference transfer, which relaxes the high demand of finding a proper reference. We adapt a joint optimization of NNF search and local color transfer across CNN layers in a hierarchical manner. We have shown that our approach is widely applicable to a variety of transfer scenarios in real-world images.

However our method still has limitations. It may mismatch some regions which exist in the source but not in the reference, and thus cause incorrect color transfer, such as the background on the left example of Figure 18. This often happens in the single-reference transfer and can be reduced by introducing more references. The VGG network we relied on cannot distinguish different instances with the same semantic labels, so it may cause color mixing be-

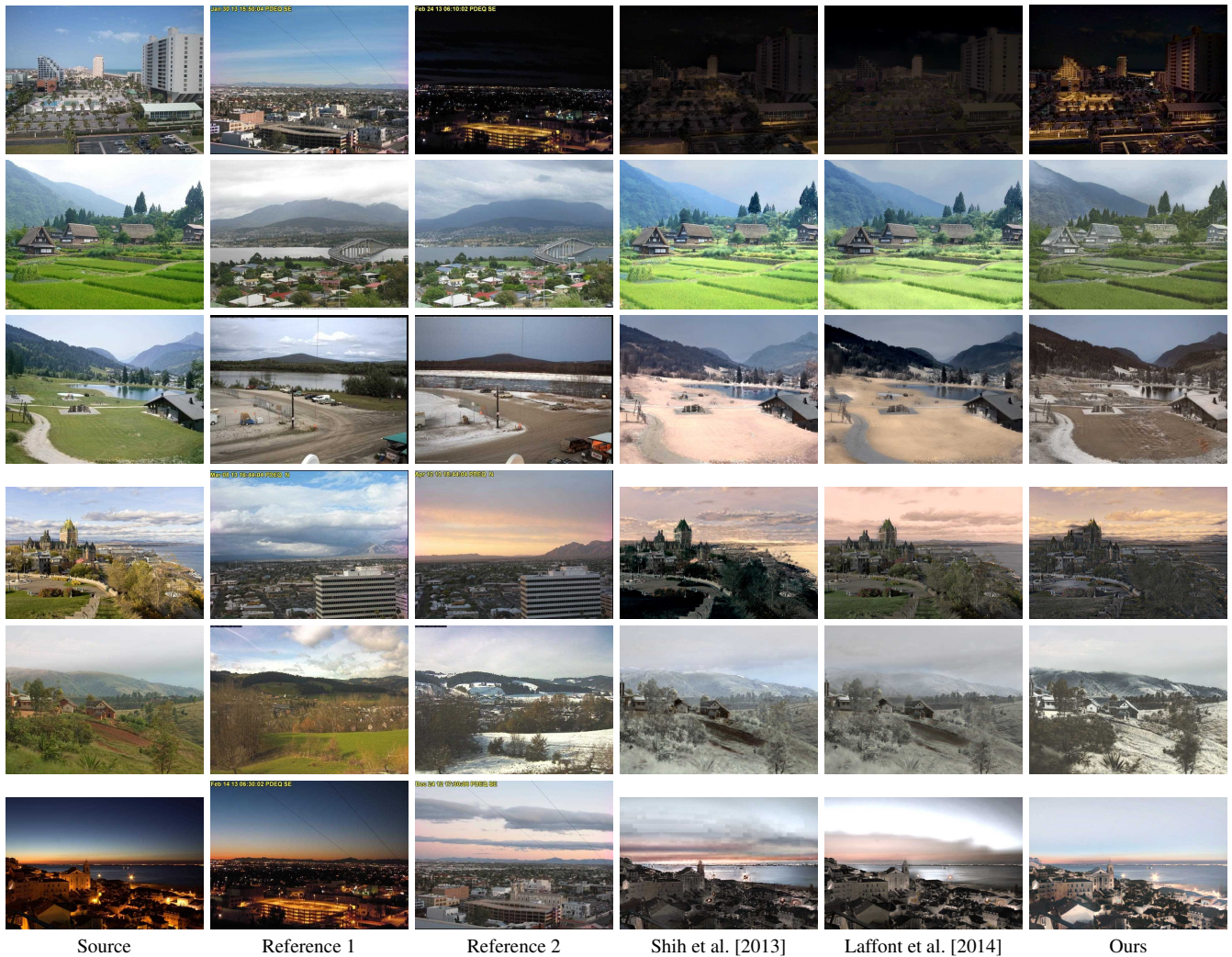


Figure 11: Comparison to local color transfer methods on the data from Laffont et al. [2014]. Shih et al. [2013] and Laffont et al. [2014] take both Reference 1 and Reference 2 as references while ours only takes Reference 1. Examples are from Laffont et al. [2014].

tween different instances, such as the man’s shirt on the right example of Figure 18, which is transferred with mixed blue and white colors from two persons in the reference. A possible improvement would be to train a network on a dataset with instance labels. Moreover, directly applying our image color transfer method to video may cause some flickering artifacts. Addressing this would require temporal constraints, and will be considered for future work.

References

- AN, X., AND PELLACINI, F. 2010. User-controllable color transfer. In *Computer Graphics Forum*, vol. 29, Wiley Online Library, 263–271.
- ARBELOT, B., VERGNE, R., HURTUT, T., AND THOLLOT, J. 2017. Local texture-based color transfer and colorization. *Computers & Graphics* 62, 15–27.
- BAE, S., PARIS, S., AND DURAND, F. 2006. Two-scale tone management for photographic look. *ACM Transactions on Graphics (TOG)* 25, 3, 637–645.
- BARNES, C., SHECHTMAN, E., FINKELSTEIN, A., AND GOLDMAN, D. 2009. Patchmatch: A randomized correspondence algorithm for structural image editing. *ACM Transactions on Graphics (TOG)* 28, 3, 24.
- CHEN, X., ZOU, D., ZHIYING ZHOU, S., ZHAO, Q., AND TAN, P. 2013. Image matting with local and nonlocal smooth priors. In *Computer Vision and Pattern Recognition (CVPR), 2013 IEEE Conference on*, 1902–1907.
- CHEN, L.-C., PAPANDREOU, G., KOKKINOS, I., MURPHY, K., AND YUILLE, A. L. 2016. Deeplab: Semantic image segmentation with deep convolutional nets, atrous convolution, and fully connected crfs. *arXiv preprint arXiv:1606.00915*.
- ENDO, Y., IIZUKA, S., KANAMORI, Y., AND MITANI, J. 2016. Deepprop: extracting deep features from a single image for edit propagation. In *Computer Graphics Forum*, vol. 35, Wiley Online Library, 189–201.
- FARBMAN, Z., FATTAL, R., LISCHINSKI, D., AND SZELISKI, R. 2008. Edge-preserving decompositions for multi-scale tone and detail manipulation. In *ACM Transactions on Graphics (TOG)*, vol. 27, 67.

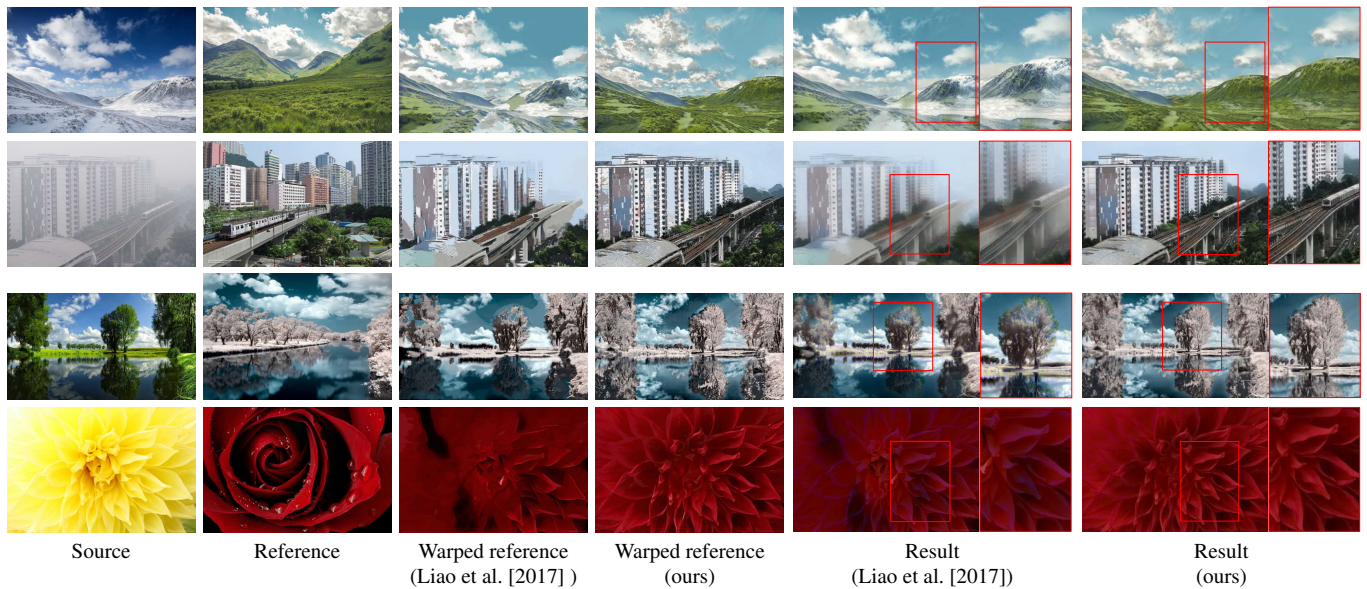


Figure 12: Compared to Liao et al. [2017], our joint optimization finds better matching (the 3rd and 4th columns) for color transfer, resulting in fewer ghosting artifacts in the color transferred result (the 5th and 6th columns). Examples are from Luan et al. [2017].

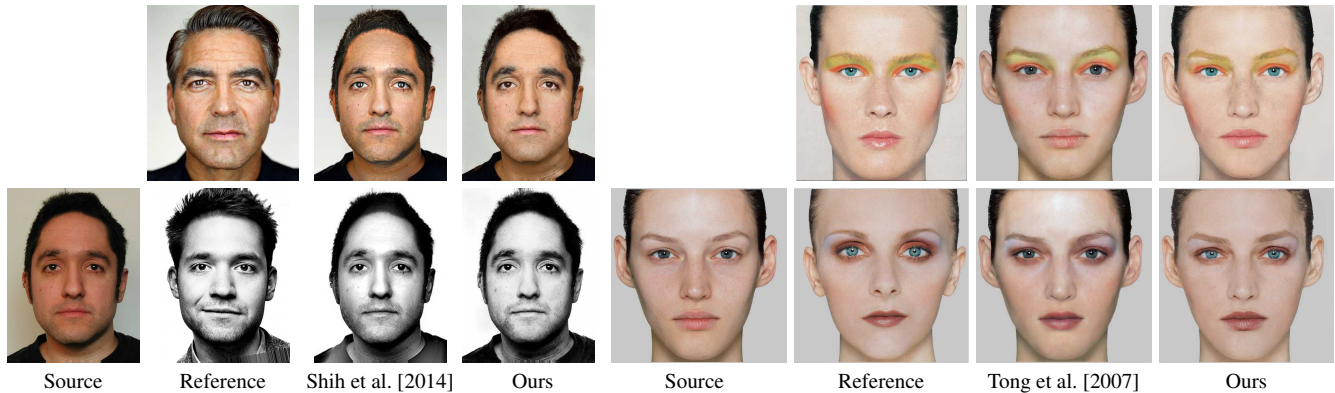


Figure 13: Comparison of portrait style transfer and cosmetic transfer. Examples are from Shih et al. [2014] (left) and Tong et al. [2007] (right).

FREEDMAN, D., AND KISILEV, P. 2010. Object-to-object color transfer: Optimal flows and smp transformations. In *Computer Vision and Pattern Recognition (CVPR), 2010 IEEE Conference on*, IEEE, 287–294.

GATYS, L. A., ECKER, A. S., AND BETHGE, M. 2015. A neural algorithm of artistic style. *arXiv preprint arXiv:1508.06576*.

HACOHEN, Y., SHECHTMAN, E., GOLDMAN, D. B., AND LISCHINSKI, D. 2011. Non-rigid dense correspondence with applications for image enhancement. *ACM transactions on graphics (TOG)* 30, 4, 70.

IZUKA, S., SIMO-SERRA, E., AND ISHIKAWA, H. 2016. Let there be color!: joint end-to-end learning of global and local image priors for automatic image colorization with simultaneous classification. *ACM Transactions on Graphics (TOG)* 35, 4, 110.

ISOLA, P., ZHU, J.-Y., ZHOU, T., AND EFROS, A. A. 2016. Image-to-image translation with conditional adversarial networks. *arXiv preprint arXiv:1611.07004*.

KHAN, A., JIANG, L., LI, W., AND LIU, L. 2016. Fast color transfer from multiple images. *arXiv preprint arXiv:1612.08927*.

KOLMOGOROV, V., AND ZABIN, R. 2004. What energy functions can be minimized via graph cuts? *IEEE transactions on pattern analysis and machine intelligence* 26, 2, 147–159.

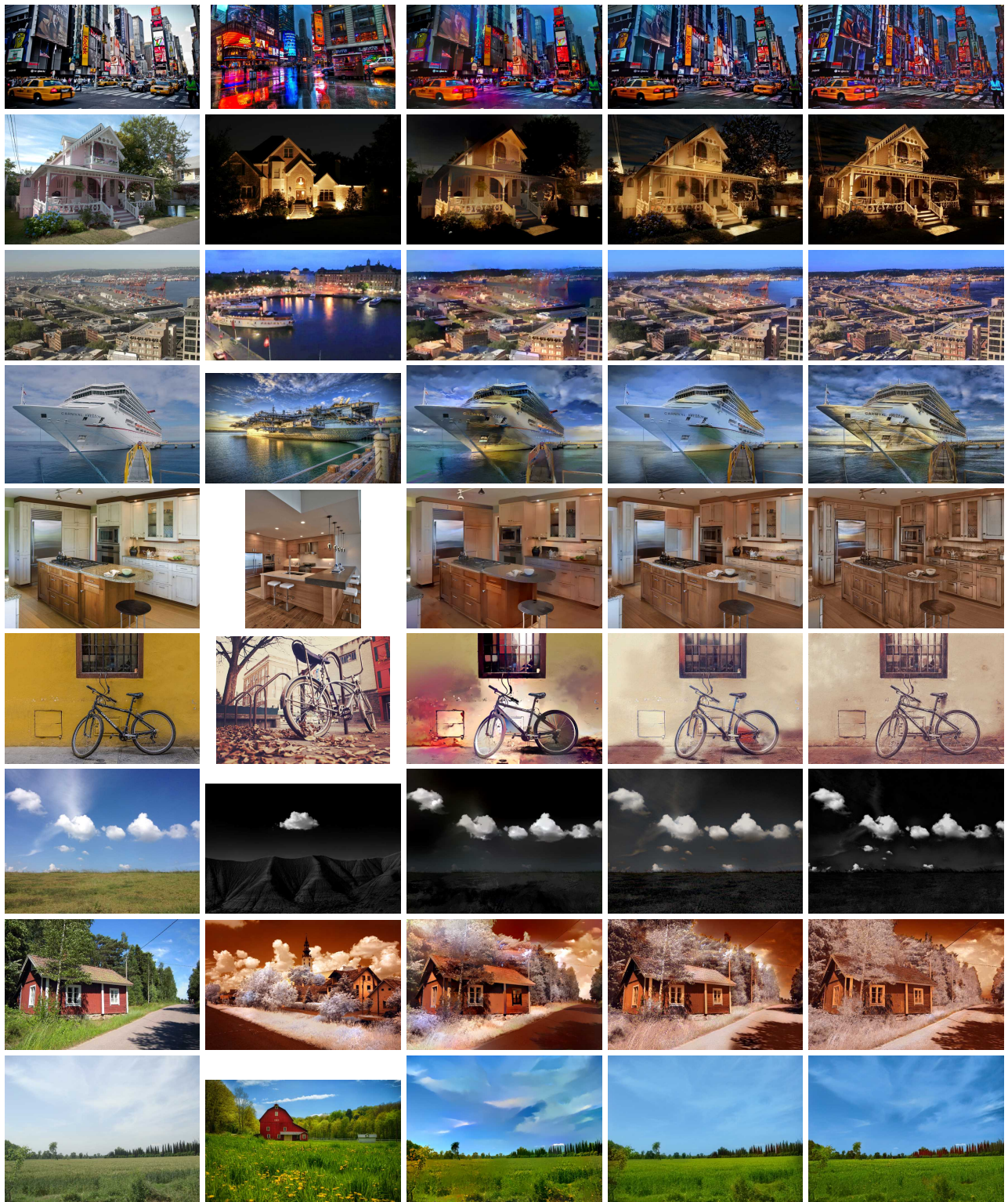
LAFFONT, P.-Y., REN, Z., TAO, X., QIAN, C., AND HAYS, J. 2014. Transient attributes for high-level understanding and editing of outdoor scenes. *ACM Transactions on Graphics (TOG)* 33, 4, 149.

LEE, J.-Y., SUNKAVALLI, K., LIN, Z., SHEN, X., AND SO KWEON, I. 2016. Automatic content-aware color and tone stylization. In *Computer Vision and Pattern Recognition (CVPR), 2016 IEEE Conference on*, 2470–2478.

LEVIN, A., LISCHINSKI, D., AND WEISS, Y. 2004. Colorization using optimization. In *ACM transactions on graphics (TOG)*, vol. 23, ACM, 689–694.

LI, C., AND WAND, M. 2016. Combining markov random fields and convolutional neural networks for image synthesis. In *Com-*

- puter Vision and Pattern Recognition (CVPR), 2016 IEEE Conference on, 2479–2486.
- LIAO, J., YAO, Y., YUAN, L., HUA, G., AND KANG, S. B. 2017. Visual attribute transfer through deep image analogy. *arXiv preprint arXiv:1705.01088*.
- LIU, Y., COHEN, M., UYTENDAELE, M., AND RUSINKIEWICZ, S. 2014. Autostyle: Automatic style transfer from image collections to users’ images. In *Computer Graphics Forum*, vol. 33, Wiley Online Library, 21–31.
- LUAN, F., PARIS, S., SHECHTMAN, E., AND BALA, K. 2017. Deep photo style transfer. *arXiv preprint arXiv:1703.07511*.
- ODENA, A., DUMOULIN, V., AND OLAH, C. 2016. Deconvolution and checkerboard artifacts. *Distill*.
- PITIE, F., KOKARAM, A. C., AND DAHYOT, R. 2005. N-dimensional probability density function transfer and its application to color transfer. In *Computer Vision, 2005. ICCV 2005. Tenth IEEE International Conference on*, vol. 2, IEEE, 1434–1439.
- REINHARD, E., ADHIKMIN, M., GOOCH, B., AND SHIRLEY, P. 2001. Color transfer between images. *IEEE Computer graphics and applications* 21, 5, 34–41.
- ROWEIS, S. T., AND SAUL, L. K. 2000. Nonlinear dimensionality reduction by locally linear embedding. *Science* 290, 2323–2326.
- RUSSAKOVSKY, O., DENG, J., SU, H., KRAUSE, J., SATHEESH, S., MA, S., HUANG, Z., KARPATHY, A., KHOSLA, A., BERNSTEIN, M., ET AL. 2015. Imagenet large scale visual recognition challenge. *International Journal of Computer Vision* 115, 3, 211–252.
- SHIH, Y., PARIS, S., DURAND, F., AND FREEMAN, W. T. 2013. Data-driven hallucination of different times of day from a single outdoor photo. *ACM Transactions on Graphics (TOG)* 32, 6, 200.
- SHIH, Y., PARIS, S., BARNES, C., FREEMAN, W. T., AND DURAND, F. 2014. Style transfer for headshot portraits. *ACM Transactions on Graphics (TOG)* 33, 4, 148:1–148:14.
- SIMAKOV, D., CASPI, Y., SHECHTMAN, E., AND IRANI, M. 2008. Summarizing visual data using bidirectional similarity. In *Computer Vision and Pattern Recognition (CVPR), 2008 IEEE Conference on*, IEEE, 1–8.
- SIMONYAN, K., AND ZISSERMAN, A. 2014. Very deep convolutional networks for large-scale image recognition. *arXiv preprint arXiv:1409.1556*.
- SUNKAVALI, K., JOHNSON, M. K., MATUSIK, W., AND PFISTER, H. 2010. Multi-scale image harmonization. *ACM Transactions on Graphics (TOG)* 29, 4, 125:1–125:10.
- TAI, Y.-W., JIA, J., AND TANG, C.-K. 2005. Local color transfer via probabilistic segmentation by expectation-maximization. In *Computer Vision and Pattern Recognition (CVPR), 2005 IEEE Conference on*, vol. 1, IEEE, 747–754.
- TONG, W.-S., TANG, C.-K., BROWN, M. S., AND XU, Y.-Q. 2007. Example-based cosmetic transfer. In *Computer Graphics and Applications, 2007. PG’07. 15th Pacific Conference on*, IEEE, 211–218.
- WELSH, T., ASHIKMIN, M., AND MUELLER, K. 2002. Transferring color to greyscale images. In *ACM Transactions on Graphics (TOG)*, vol. 21, ACM, 277–280.
- YAN, Z., ZHANG, H., WANG, B., PARIS, S., AND YU, Y. 2016. Automatic photo adjustment using deep neural networks. *ACM Transactions on Graphics (TOG)* 35, 2, 11.
- YOO, J.-D., PARK, M.-K., CHO, J.-H., AND LEE, K. H. 2013. Local color transfer between images using dominant colors. *Journal of Electronic Imaging* 22, 3, 033003–033003.
- ZHANG, R., ISOLA, P., AND EFROS, A. A. 2016. Colorful image colorization. In *European Conference on Computer Vision (ECCV), 2016*, Springer, 649–666.
- ZHAO, Q., TAN, P., DAI, Q., SHEN, L., WU, E., AND LIN, S. 2012. A closed-form solution to retinex with nonlocal texture constraints. *IEEE transactions on pattern analysis and machine intelligence* 34, 7, 1437–1444.
- ZHU, J.-Y., PARK, T., ISOLA, P., AND EFROS, A. A. 2017. Unpaired image-to-image translation using cycle-consistent adversarial networks. *arXiv preprint arXiv:1703.10593*.



Source Reference Luan et al. [2017] Liao et al. [2017] Ours

Figure 14: Comparison to recent color transfer methods based on deep features. Examples are from [Luan et al. 2017].

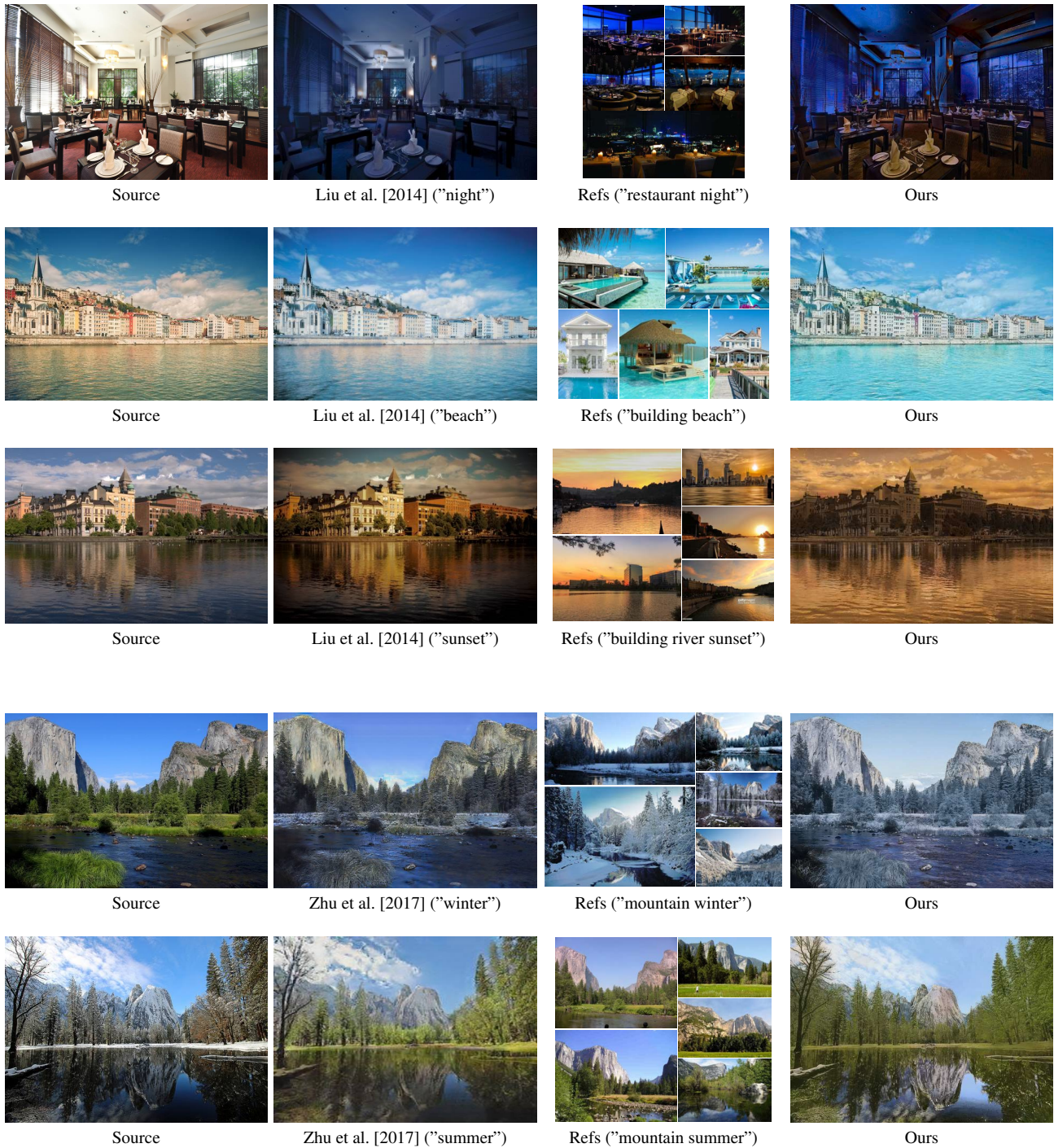


Figure 15: Comparison with multiple color transfer methods on their source images and our own references automatically searched from the Internet based on the keywords. Sources are from Liu et al. [2014] (top three) and Zhu et al. [2017] (bottom two).

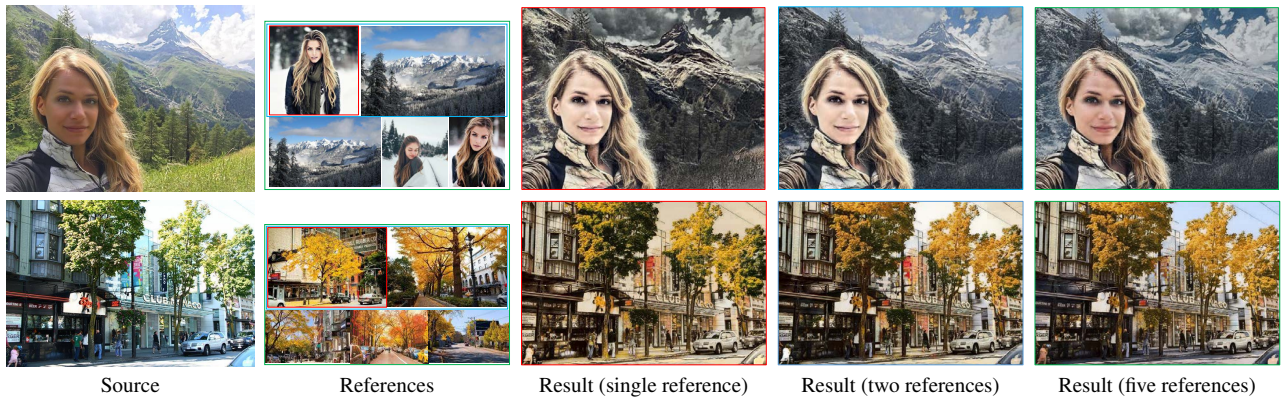


Figure 16: Comparison of our method with single and multiple references. Please note that references with the same boundary color as the result are used to generate this result.



Figure 17: Colorization Results.



Figure 18: Failure cases.